Konrad-Zuse-Zentrum
für Informationstechnik Berlin

Takustraße 7
D-14195 Berlin-Dahlem
Germany

DANIEL RUPRECHT ACHIM SCHÄDLE
FRANK SCHMIDT LIN ZSCHIEDRICH

Transparent boundary conditons for time-dependent problems

ZIB-Report 07-12 (Mai 2007)

TRANSPARENT BOUNDARY CONDITONS FOR TIME-DEPENDENT PROBLEMS

DANIEL RUPRECHT*, ACHIM SCHÄDLE*, FRANK SCHMIDT*, AND LIN ZSCHIEDRICH*

Abstract. A new approach to derive transparent boundary conditions (TBCs) for wave, Schrödinger, heat and drift-diffusion equations is presented. It relies on the pole condition and distinguishes between physical reasonable and unreasonable solutions by the location of the singularities of the spatial Laplace transform of the exterior solution. To obtain a numerical algorithm, a Möbius transform is applied to map the Laplace transform onto the unit disc. In the transformed coordinate the solution is expanded into a power series. Finally, equations for the coefficients of the power series are derived. These are coupled to the equation in the interior, and yield transparent boundary conditions. Numerical results are presented in the last section, showing that the error introduced by the new approximate TBCs decays exponentially in the number of coefficients.

Key words. transparent boundary condition, non-reflecting boundary condition, pole condition, wave equation, Schrödinger equation, drift diffusion equation

AMS subject classifications. 65M60 65M20 30E10

1. Introduction.

In the simulation of wave propagation phenomena on unbounded domains transparent boundary conditions are needed in order to make the computational domain finite.

Here we present a new concept based on the pole condition to derive transparent boundary conditions for the wave equation, the Schrödinger equation and the drift-diffusion equation. The symbol $p(\partial_t)$ is used to treat all the equations simultaneously:

$$p(\partial_t)u(t,x) = \partial_{xx}u(t,x) + 2d\partial_x u(t,x) - k^2(t,x)u(t,x) \text{ for } x \in \mathbb{R},\ t \geq 0. \qquad (1.1)$$

The pole condition as presented here is reduced to the condition that some function $U(s,t)$ is analytic on the unit disk. Expanding $U(s,t)$ into a power series $\sum_{\ell=0}^{\infty} a_\ell(t)s^\ell$ a system of ordinary differential equations for the coefficients $a_\ell(t)$ is deduced, that is coupled to the boundary data of u. Truncating the power series yields an algorithm to realize transparent boundary conditions.

The pole condition approach shares the variational formulation with transparent boundary conditions based on infinite elements [2] but is nevertheless distinctively different. In the derivation of the pole condition, ansatz and test functions are different and the ansatz functions do not represent a meaningful solution in the exterior. The pole condition is similar to the perfectly matched layer method [3], which does not give a representation of the solution in the exterior either. In contrast to the PML method the pole condition method does not rely on a damping of plane waves in the exterior by introducing a complex coordinate stretching [4]. Hence the pole condition method is also applicable to e.g. drift diffusion equations.

The exact transparent boundary conditions, which are reviewed briefly in Section 2 are non-local in time. For a special choice of parameters our approach coincides with the exact transparent boundary conditions. However one can choose parameters such that the boundary conditions become local in time.

*ZIB Berlin, Takustr. 7, D-14195 Berlin, Germany. E-mail: schaedle@zib.de. Supported by the DFG Research Center MATHEON "Mathematics for key technologies" in Berlin.

The paper is organized is follows: In Section 2 the problem class is introduced and classical transparent boundary conditions are described. Section 3 describes in detail the derivation of the newly developed transparent boundary conditions, which are based on the pole condition. Section 4 describes the spacial discretization and Section 5 the time discretization. Section 6 finally gives numerical results for all four equations.

2. Problem class and classical transparent boundary conditions. In this section we introduce the problem class. Classical transparent boundary conditions are described and we comment on their implementation very briefly.

For a more detailed discussion on transparent boundary conditions the reader is referred to excellent reviews [6, 7] and [18].

The generic equation (1.1) includes the wave equation (2.1), the drift-diffusion equation (2.2), the heat equation (2.2) with $d = 0$ and the Schrödinger equation (2.3). The exact transparent boundary condition for these equations are well established in the literature.

$$\partial_{tt} u(t,x) = \partial_{xx} u(t,x) - k^2(t,x) u(t,x) \text{ for } x \in \mathbb{R},\ t \geq 0, \tag{2.1}$$

$$\partial_t u(t,x) = \partial_{xx} u(t,x) + 2d\partial_x u(t,x) - k^2(t,x) u(t,x) \text{ for } x \in \mathbb{R},\ t \geq 0, \tag{2.2}$$

$$i\partial_t u(t,x) = \partial_{xx} u(t,x) - k^2(t,x) u(t,x) \text{ for } x \in \mathbb{R},\ t \geq 0. \tag{2.3}$$

These equations have to be complemented with appropriate initial conditions. $k(x,t)$ and d are assumed to be real. Furthermore $k(x,t)$ is assumed to be constant outside the space-time strip $(x,t) \in \Omega_t = [-a,a] \times [0,\infty)$ and initial values are assumed to be compactly supported in $[-a,a]$.

2.1. Derivation of transparent boundary conditions. Suppose one is only interested in the solution within the strip Ω_t and let v denote the restriction of u to Ω_t. To obtain an equation for v boundary conditions along the artificial boundary $\Gamma_t = \{-a,a\} \times [0,\infty)$ are needed, such that the solution of (1.1) (defined on $\mathbb{R} \times [0,\infty)$) coincides with v on Ω_t. To derive such transparent boundary conditions denote by w the restriction of u to the exterior $\Omega_t^C = \{(-\infty,-a] \cup [a,\infty)\} \times [0,\infty)$.

A Laplace transformation of w in t with dual variable ω, where the transformed function is denoted by $\mathbf{w} = \mathcal{T}(w)$, i.e.

$$\mathbf{w}(\omega) = \mathcal{T}(w)(\omega) = \int_0^\infty \mathrm{e}^{\omega t} w(t) dt$$

yields

$$p(\omega)\mathbf{w}(\omega,x) = \partial_{xx}\mathbf{w}(\omega,x) + 2d\partial_x \mathbf{w}(\omega,x) - k^2 \mathbf{w}(\omega,x) \text{ for } |x| > a, \tag{2.4}$$

$$\mathbf{w}(\omega,x) = \mathbf{v}(\omega,x) \text{ for } |x| = a. \tag{2.5}$$

Equation (2.4) is obtained taking into account that the initial value(s) vanish and k is constant outside Ω_t. The Laplace transform is defined in some right half plane of the complex plane. Assuming that $\Re(\omega) > 0$ and choosing the branch of the square root such that $\Re\left((p(\omega) + d^2 + k^2)^{1/2}\right) > 0$, Equation (2.4) has only one bounded solution that solves the problem:

$$\begin{aligned} \mathbf{w}(\omega,x) = &\quad C e^{\left(-d-(p(\omega)+k^2+d^2)^{1/2}\right)x} \quad \text{for } x > a, \\ \mathbf{w}(\omega,x) = &\quad C e^{\left(-d+(p(\omega)+k^2+d^2)^{1/2}\right)x} \quad \text{for } x < -a. \end{aligned} \tag{2.6}$$

For the Schrödinger equation it is $d = 0$ and thus $p(\omega)$ has non-negative imaginary part and so has $p(\omega) + k^2$. Hence $(p(\omega) + k^2)^{1/2}$ takes values in the first quadrant of the complex plane. The solutions given in (2.6) are either decaying exponentially or obey the Sommerfeld radiation condition, i.e they are outward radiating.

For the drift-diffusion and the heat equation $p(\omega)$ has non-negative real part. For all $d,\ k \in \mathbb{R}$ it holds that $-d-(k^2+d^2)^{1/2} \leq 0$ and $-d+(k^2+d^2)^{1/2} \geq 0$. Thus the real part of $-d-(p(\omega)+k^2+d^2)^{1/2}$ is negative and the real part of $-d+(p(\omega)+k^2+d^2)^{1/2}$ is positive. The solutions given above are hence decaying exponentially.

As the wave equation is time reversible, we assume that ω is purely imaginary. This formally corresponds to a Fourier transform from $t = -\infty$ to $t = \infty$ instead of a Laplace transform along $[0, \infty)$. Having $d = 0$, $(p(\omega) + k^2)^{1/2}$ takes values on the imaginary semi-axis or on an interval on the real line, i.e. in $\{iy : y \in \mathbb{R}_+\} \cup [0, k]$. Again, the solutions are either decaying exponentially or obey the Sommerfeld radiation condition.

The constant C is chosen such that the boundary condition (2.5) is fulfilled. Inserting the normal derivatives $\partial_\nu v(t,-a) = -\partial_x v(t,-a), \quad \partial_\nu v(t,a) = \partial_x v(t,a)$ into the equation for v, the solution in the interior is obtained from

$$\begin{aligned} p(\partial_t)v(t,x) &= v_{xx}(t,x) + 2dv(t,x) - k^2 v(t,x) \text{ for } x \in\ I,\ t \geq 0 \\ \partial_\nu v(t,\pm a) &= -\partial_\nu w(t,\pm a) = \mathcal{T}^{-1}\left(\left(\mp d - (p(\cdot)+k^2+d^2)^{1/2}\right)\mathcal{T}(v(\cdot,\pm a))\right)(t) \\ &= \int_0^t \mathcal{T}^{-1}\left(\mp d - (p(\cdot)+k^2+d^2)^{1/2}\right)(t-\tau)v(\tau,\pm a)d\tau. \end{aligned} \tag{2.7}$$

Alternatively one obtains

$$\begin{aligned} p(\partial_t)v(t,x) &= v_{xx}(t,x) + 2dv_x(t,x) - k^2 v(t,x) \text{ for } x \in\ I,\ t \geq 0 \\ v(t,\pm a) &= \mathcal{L}^{-1}\left(\left(\mp d - (p(\cdot)+k^2)^{1/2}\right)^{-1}\mathcal{T}(\partial_\nu v(\cdot,\pm a))\right)(t) \\ &= \int_0^t \mathcal{T}^{-1}\left(\left(\mp d - (p(\cdot)+k^2+d^2)^{1/2}\right)^{-1}\right)(t-\tau)\partial_\nu v(\tau,\pm a)d\tau. \end{aligned} \tag{2.8}$$

As is seen from (2.7) and (2.8) transparent boundary conditions are in general of convolution type. The discretization of (2.8) with respect to time is not straightforward and may introduce instabilities. A stable discretization is obtained using convolution quadrature [11, 12], based on the same time integration scheme as used in the interior. It is shown in [14] that this is equivalent to the derivation of time-discrete transparent boundary conditions given below.

2.2. Derivation of time discrete transparent boundary conditions. The equation for u (1.1) is discretized in time using an A-stable multi-step method, such as the trapezoidal rule. Time discrete transparent boundary conditions are now derived following almost the same procedure as above. The only difference is that instead of applying a Laplace transform in the variable t a Z-transform is applied.

$$\mathbf{u}(\zeta) := \mathcal{Z}(u)(\zeta) := \sum_n u(nh)\zeta^n$$

Denoting by $\delta(\zeta)$ [1] the generating function of the multi-step method, the time-discrete transparent boundary condition is

$$v(nh, \pm a) = \mathcal{Z}^{-1}\left(\mp d - (p(\delta(\cdot)/h) + k^2 + d^2)^{-1/2}\mathcal{Z}(v)(\cdot)\right)(n) = \sum_{j=0}^{n} w_{n-j}\partial_\nu v_j, \tag{2.9}$$

where the convolution weights w_n are given by the power series expansion

$$\mp d - (p(\delta(\zeta)/h) + k^2 + d^2)^{-1/2} = \sum_j w_j \zeta^j \ . \tag{2.10}$$

The timediscrete transparent boundary condition (2.9) has the same structure as (2.8).

In general the weights have to be calculated numerically. To calculate N weights with precision ε the complexity is is $\mathcal{O}(N \log N \varepsilon \log(\varepsilon))$, c.f. [12, Sec. 7]. In our simple setting it should however be possible for the trapezoidal rule to calculate the weights analytically, see e.g. [1, 17].

In the derivation of the exact transparent boundary conditions in Sections 2.1 and 2.2 it was *necessary* after applying a Laplace- or Z-transform to solve the second order differential equation in x, and to chose among two linear independent solutions the one that has the correct asymptotic behavior for $x \to \infty$. For higher spatial dimensions however this is, if at all, only possible in very special cases. In what follows we present a more general concept, that avoids solving ODEs and picking certain solutions. The basis for this is the pole condition approach proposed by Schmidt in [15, 9, 16].

3. An alternative derivation of transparent boundary conditions. The basic idea of the pole condition is to test the exterior solution against any incoming field $\exp(sx)$ by trying to evaluate $\int_a^\infty u(x)\exp(sx)$. This integral will diverge in case $u(x)$ has incoming components. What is incoming and outgoing is now determined by the phase of the test function $\exp(sx)$, i.e. by the complex value s. The situation will be analyzed for each type of equation in Section. 3.2.

3.1. Variational formulation. The starting point is the Laplace transform in t of (1.1)

$$p(\omega)\mathbf{u}(\omega, x) = \partial_{xx}\mathbf{u}(\omega, x) + 2d\partial_x\mathbf{u}(\omega, x) - K(\mathbf{u}) \tag{3.1}$$

Here the term $K(\mathbf{u})$ is the Laplace transform of the $k(x,t)u(x,t)$ and additionally contains the initial value(s). Multiplying by a test function v and integrating over $\mathbb{R}$ the variational form is given by: Find $u \in H^1(\mathbb{R})$ such that

$$\int_{\mathbb{R}} p(\omega)\mathbf{u}(\omega, x)v(x)\,dx = \int_{\mathbb{R}} -\mathbf{u}_x(\omega, x)v_x(x) + 2d\mathbf{u}_x(\omega, x)v(x) - K(\mathbf{u})v(x)\,dx \tag{3.2}$$

for all $v \in H^1(\mathbb{R})$. ω may be considered to be the dual variable with respect to t or the generating function $\delta(\zeta)$. It is sufficient to test against all v in some dense

[1] In case of the trapezoidal rule $\delta(\zeta) = 2\frac{1+\zeta}{1-\zeta}$. For the implicit Euler method $\delta(\zeta) = \frac{1}{1-\zeta}$. In general δ is the quotient of the generating polynomials [8, III.2]. An Extension to Runge Kutta methods is possible [13].

subset and we will use that freedom and restrict to the set of all $v \in H^1(\mathbb{R})$, such that $v(x) = ce^{-s(x-a)}$ for $x > a$ and $v(x) = ce^{s(x+a)}$ for $x < -a$, with $\Re s > 0$ and $c \in \mathbb{C}$. The set of test functions can be restricted even further to those satisfying $c = 1$. Splitting the integral in (3.2) one obtains

$$\begin{aligned}&\int_{[-a,a]} p(\omega)\mathbf{u}(\omega,x)v(x)\,dx + \int_{|x|>a} p(\omega)\mathbf{u}(\omega,x)v(x)\,dx = \\ &\int_{[-a,a]} -\mathbf{u}_x(\omega,x)v_x(x) + 2d\mathbf{u}_x(\omega,x)v(x) - K(\mathbf{u})v(x)\,dx + \\ &\int_{|x|>a} -\mathbf{u}_x(\omega,x)v_x(x) + 2d\mathbf{u}_x(\omega,x)v(x) - k^2\mathbf{u}(\omega,x)v(x)\,dx.\end{aligned} \tag{3.3}$$

Note that v has to be equal to 1 at $x = \pm a$ and that $\mathbf{u}(\omega, \pm a \pm h) = \mathbf{u}(\omega, \pm a \mp h)$. for $h \to 0$. Inserting the special form of v outside $[-a, a]$ one obtains

$$\begin{aligned}&\int_{[-a,a]} p(\omega)\mathbf{u}(\omega,x)v(x)\,dx + p(\omega)U^{(l)}(\omega,s) + p(\omega)U^{(r)}(\omega,s) = \\ &\int_{[-a,a]} -\mathbf{u}_x(\omega,x)v_x(x) + 2d\mathbf{u}_x(\omega,x)v(x) - K(\mathbf{u})v(x)\,dx \\ &+ s(sU^{(l)}(\omega,s) - \mathbf{u}(\omega,-a)) - 2d(sU^{(l)}(\omega,s) - \mathbf{u}(\omega,-a)) - k^2U^{(l)}(\omega,s) \\ &+ s(sU^{(r)}(\omega,s) - \mathbf{u}(\omega,a)) + 2d(sU^{(r)}(\omega,s) - \mathbf{u}(\omega,a)) - k^2U^{(r)}(\omega,s),\end{aligned} \tag{3.4}$$

where

$$U^{(r)}(\omega,s) = \int_a^\infty \mathbf{u}(\omega,x)\mathrm{e}^{-s(x-a)}\,dx = \int_0^\infty \mathbf{u}(\omega,x+a)\mathrm{e}^{-sx}\,dx,$$

$$U^{(l)}(\omega,s) = \int_{-\infty}^{-a} \mathbf{u}(\omega,x)\mathrm{e}^{s(x+a)}\,dx = \int_0^\infty \mathbf{u}(\omega,-x-a)\mathrm{e}^{-sx}\,dx$$

are the Laplace transforms of the solution in the exterior. Transparent boundary conditions may be now be set by imposing appropriate conditions on $U^{(l,r)}$, c.f. Section 3.2.

Classical transparent boundary conditions are connecting Neumann and Dirichlet data at the boundary. A reinterpretation of (3.4) will supply the Neumann data at the boundary. Suppose a function u on $I = [-a, a]$ is given obeying (3.1). Multiplying by a test function and integrating by parts yields

$$\begin{aligned}\int_I p(\omega)\mathbf{u}(\omega,x)v(x)dx = \int_I &-\partial_x\mathbf{u}(\omega,x)\partial_x v(x)dx + 2d\partial_x\mathbf{u}(\omega,x)v(x) - K(\mathbf{u})v(x)dx \\ &+ \partial_x\mathbf{u}(\omega,a)v(a) - \partial_x\mathbf{u}(\omega,-a)v(-a).\end{aligned}$$

Choosing a test function that vanishes at $-a$ and is 1 at a the above equation allows to weakly define the outward normal derivative of $\mathbf{u}(\omega, a)$ at $x = a$ by

$$\partial_x\mathbf{u}(\omega,a)v(a) = \int_I p(\omega)\mathbf{u}(\omega,x)v + \partial_x\mathbf{u}(\omega,x)\partial_x v - 2d\partial_x\mathbf{u}(\omega,x)v + K(\mathbf{u})vdx$$

and similarly for the outward normal derivative of $\mathbf{u}(\omega, -a)$ at $x = -a$

$$-\partial_x\mathbf{u}(\omega,a)v(a) = \int_I p(\omega)\mathbf{u}(\omega,x)v + \partial_x\mathbf{u}(\omega,x)\partial_x v - 2d\partial_x\mathbf{u}(\omega,x)v + K(\mathbf{u})vdx.$$

3.2. Pole condition. Suppose the Laplace transform in the exterior U as function of s has some singularities in the complex plane. By Cauchy's integral formula

$$U(s) = \frac{1}{2\pi i} \int_\gamma (s-\tau)^{-1} U(\tau) d\tau$$

where γ is a path enclosing the singularities of U. This path integral may be interpreted as a superposition of $(s-\tau)^{-1}$. This is easily seen by inserting the Riemann sum for the path integral, which gives

$$U(s) = \lim_{N\to\infty} \sum_{j=1}^{N} b_j(N, U(\tau_j)) \frac{1}{s-\tau_j}$$

for weights b_j. Transforming back to space domain we have the correspondence

$$\frac{1}{s-\tau} \leftrightarrow \mathrm{e}^{x\tau}$$

Depending on the location of τ in the complex plane, $\mathrm{e}^{x\tau}$ is outward radiating/expotentially decreasing or incoming/exponentially increasing. This way the complex plane can be divided into two regions; a region $\mathbb{C}^{\text{in}} = \{\tau \in \mathbb{C} : \mathrm{e}^{x\tau} \text{ is incoming } \}$ and a region $\mathbb{C}^{\text{out}} = \{\tau \in \mathbb{C} : \mathrm{e}^{x\tau} \text{ is outward radiating } \}$. Now split the contour γ in two contours γ_{in} and γ_{out} where γ_{in} lies in $\mathbb{C}^{\text{in}}$ and encloses all singularities of U in this region. while γ_{out} lies in $\mathbb{C}^{\text{out}}$ enclosing all singularities in this region. The integral over γ is then decomposed as follows

$$U(s) = \int_{\gamma_{in}} (s-\tau)^{-1} U(\tau) d\tau + \int_{\gamma_{out}} (s-\tau)^{-1} U(\tau) d\tau.$$

Requiring that $\mathbf{u}(\omega, x)$ is purely outward radiating is now equivalent to the condition $\int_{\gamma_{in}} (s-\tau)^{-1} U(\tau) d\tau = 0$, which in turn is equivalent to the condition that $U(s)$ is analytic in $\mathbb{C}^{\text{in}}$. We can summarize this in the following definition.

Definition 3.1 (Pole condition). *A solution $\mathbf{u}(\omega, x)$ obeys the pole condition if the Laplace transform $U(\omega, s)$ is analytic in $\mathbb{C}^{\text{in}}$.*

The equivalence of the pole condition with the Sommerfeld radiation condition for the two dimensional Helmholtz equation for a homogenous exterior domain was proven in [9]. What these regions $\mathbb{C}^{\text{out}}$ and $\mathbb{C}^{\text{in}}$ look like is discussed in Sections 3.2.1 to 3.2.4 for the different type of equations.

The above reasoning can be made more explicit for the simple one-dimensional model problem. It is stressed however that for the construction of the transparent boundary condition the following explicit calculations are not necessary. They are presented to give the reader some confidence in the method and to show how classical transparent boundary conditions are contained as a special case.

Suppose for the moment $\mathbf{u}$ is given on $[-a, a]$ and consider the right exterior only. The equation for $U^{(r)}$ is then

$$-p(\omega) U^{(r)}(\omega, s) + s^2 U^{(r)}(\omega, s) + 2ds U^{(r)}(\omega, s) - k^2 U^{(r)}(\omega, s) = r(s, \mathbf{u})$$

with the remainder term

$$r(s, \mathbf{u}) = \partial_x \mathbf{u}(\omega, a) v(a) + 2d\mathbf{u}(\omega, a) + s\mathbf{u}(\omega, a)$$

which is analytic in s. Solving for $U^{(r)}$ we obtain

$$U^{(r)}(\omega, s) = \left(s^2 + 2ds - (p(\omega) + k^2)\right)^{-1} r(s, \mathbf{u}). \tag{3.5}$$

For fixed ω there are always two roots s_- and s_+ of $s^2 + 2ds - (p(\omega) + k^2)$, so U can be decomposed as follows

$$U^{(r)}(\omega, s) = (s - s_+)^{-1} r_1(\omega, \mathbf{u}) + (s - s_-)^{-1} r_2(\omega, \mathbf{u}). \tag{3.6}$$

with

$$r_1(\omega, \mathbf{u}) = \frac{1}{2}\left(\mathbf{u}(\omega, a) + \frac{\partial_x \mathbf{u}(\omega, a) v(a) + 2d\mathbf{u}(\omega, a)}{\sqrt{p(\omega) + k^2 + d^2}}\right)$$

and

$$r_2(\omega, \mathbf{u}) = \frac{1}{2}\left(\mathbf{u}(\omega, a) - \frac{\partial_x \mathbf{u}(\omega, a) v(a) + 2d\mathbf{u}(\omega, a)}{\sqrt{p(\omega) + k^2 + d^2}}\right)$$

Transforming back to space domain the summands in (3.6) correspond to solutions $\exp(xs_+)$ and $\exp(xs_-)$. Depending on the location of $s_\pm$ in the complex plane incoming and outgoing, exponentially decaying and exponentially increasing solutions can be identified. A similar splitting is obtained for the left boundary.

The possible location of the poles s_+ and s_- for the four different equations is considered more closely in Sections 3.2.1 to 3.2.4. It is then argued how to construct boundary conditions that in the case of the Schrödinger and the wave equation distinguish incoming and outgoing waves. In case of the drift diffusion equation the boundary condition distinguishes between bounded (physical reasonable) and unbounded (unphysical) solutions.

3.2.1. Heat equation. If $p(\omega) = \omega$, where ω takes values in the right half plane, then $p(\omega) + k^2$ is shifted by k^2. The roots of $s^2 - (p(\omega) + k^2)$ take values in regions to the left and right of the imaginary axis that are bounded by hyperbolas as sketched in the right plot in Fig. 3.1. Clearly the roots to the right correspond to unphysical exponentially increasing solutions. To exclude these, one requires that $U(\omega, s)$ is analytic in the right half plane.

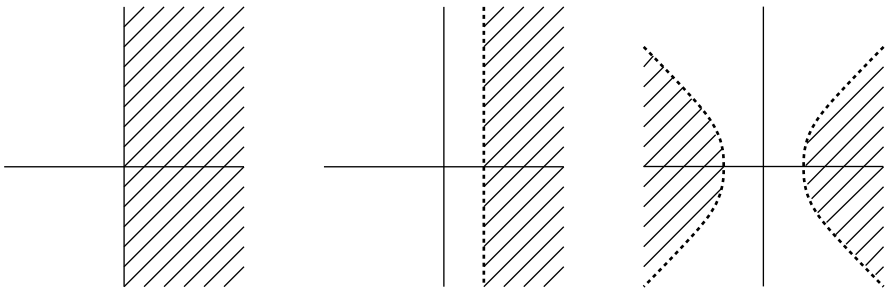

FIG. 3.1. *Left: possible values of $p(\omega)$. Middle: possible values of $p(\omega) + k^2$. Right: location of the roots $s_\pm$. To each root in the left region there corresponds one root in the right region.*

3.2.2. Schrödinger equation. If $p(\omega) = i\omega$, where ω takes values in the right half plane, then $p(\omega) + k^2$ is rotated counter clockwise by $\pi/4$ and shifted by k^2. Thus $p(\omega) + k^2$ attains values in the upper half plane as sketched in the middle plot of Fig 3.2. The roots of $s^2 - (p(\omega) + k^2)$ take values in first and third quadrant as sketched in the right plot in Fig. 3.2. The roots in the first quadrant correspond to unphysical solutions, that are either exponentially increasing or have the wrong phase shift. To exclude these one may for instance require that $U(\omega, s)$ is analytic in the upper-right half plane bounded by the bisecting line of the second and fourth quadrant.

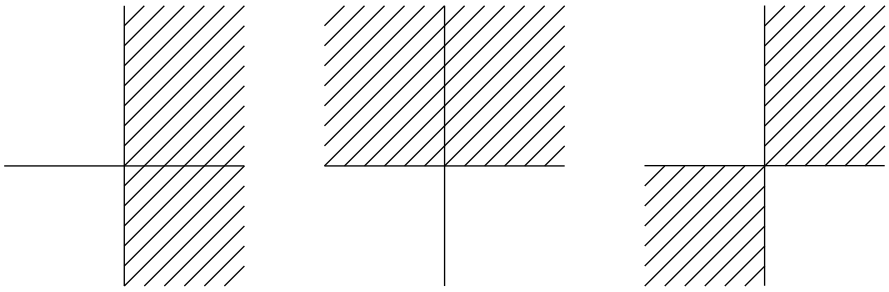

FIG. 3.2. *Left: possible values of $p(\omega)$. Middle: possible values of $p(\omega) + k^2$. Right: location of the roots $s_\pm$. To each root in the first quadrant there corresponds one root in the third quadrant.*

3.2.3. Wave equation. If $p(\omega) = \omega^2$, $p(\omega) + k^2$ takes values everywhere. The imaginary axis is mapped to the axis $\{\Im s = 0\,; \Re s < k^2\}$. The roots now fill the whole complex plane. The values along the cross as indicated in the right plot of Fig. 3.3 correspond to the axis $\{\Im s = 0\,; \Re s < k^2\}$. Solutions corresponding to roots in the lower half plane are incoming, transformed back to space domain they do not satisfy the Sommerfeld radiation condition.

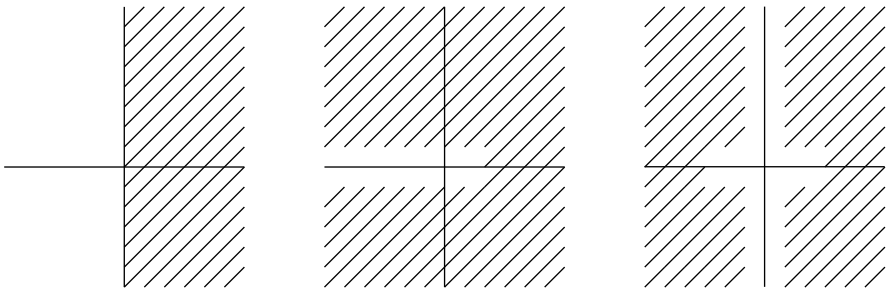

FIG. 3.3. *Left: possible values of $p(\omega)$. Middle: possible values of $p(\omega) + k^2$. Right: location of the roots $s_\pm$.*

3.2.4. Drift diffusion equation. If $p(\omega) = \omega$, where ω takes values in the right half plane, then $p(\omega)+k^2$ is shifted by k^2. The roots of $s^2+2ds-(p(\omega)+k^2)$ take values in regions to the left and right of the imaginary axis that are bounded by hyperbolas as sketched in the right plot in Fig. 3.4. Clearly the roots to the right correspond to unphysical exponentially increasing solutions. In the drift diffusion example the position of the roots is different for the left and right boundary, they are symmetric with the respect to the $\Re s = \pm D$ for the left and right boundary respectively. To

exclude the roots in the right region one requires that $U(\omega, s)$ is analytic in right half plane, bounded by the axis $\Re s = \pm D$.

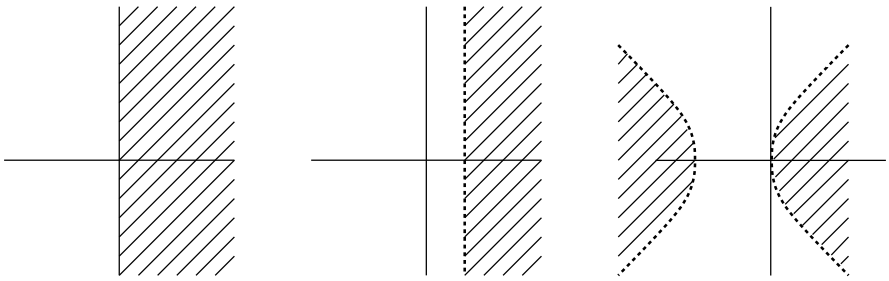

FIG. 3.4. *Left: possible values of $p(\omega)$. Middle: possible values of $p(\omega) + k^2$. Right: location of the roots $s_\pm$. To each root in the left region there corresponds one root in the right region.*

Calculating the roots $s_\pm$ and the functions r_1 and r_2 for each of the above cases this means that

$$\mathbf{u}(\omega, a) + \frac{\partial_\nu \mathbf{u}(\omega, a) v(a)}{\sqrt{p(\omega) + k^2}} = 0 \text{ equivalently } \sqrt{p(\omega) + k^2}\mathbf{u}(\omega, 0) + \partial_\nu \mathbf{u}(\omega, a) v(a) = 0$$

which is equivalent to the boundary conditions given in (2.8), (2.9) and (2.7).

3.3. The pole condition in Hardy space. We will now reformulate the boundary condition in a way that will allow an easy implementation. For this we map the domain where $U(s)$ is required to be analytic to the unit disc. With this change of coordinates, the condition on U to be analytic in some half plane is now formulated as condition on U to be analytic on the unit disk. In the new coordinate U may then be expanded into a power series.

The mapping is done by a Möbius transformation which in general form is given by

$$\Phi : s \mapsto \tilde{s} = \frac{\alpha s + \beta}{\gamma s + \delta} \tag{3.7}$$

In case of the heat, wave and Schrödinger equation we set $\alpha = \gamma = 1$, $\beta = s_0(\omega)$ and $\delta = -s_0(\omega)$, such that the Möbius transform maps the half plane

$$\{z : \Re(-z/s_0(\omega)) \leq 0\} \tag{3.8}$$

onto the unit disk. The point $-s_0(\omega)$ is mapped to 0. The inverse transform is given by

$$\Phi^{-1} : \tilde{s} \mapsto s = \frac{a\tilde{s} + b}{c\tilde{s} + d} = s_0(\omega)\frac{\tilde{s} + 1}{\tilde{s} - 1} \tag{3.9}$$

This justifies the following ansatz for $U(\omega, \tilde{s})$

$$U(\omega, \tilde{s}) = \sum_{\ell=0}^{\infty} a_n(\omega)\tilde{s}^n \tag{3.10}$$

In case of the drift-diffusion equation the two regions with the poles are symmetric with respect the axis parallel to the imaginary axis but shifted by $\pm D$ for the right

and left boundary respectively. Thus different Möbius transforms are used for the left and right boundary. We set for the right boundary $a^{(r)} = (d - s0)$, $b^{(r)} = -(d + s0)$, $c^{(r)} = -1$, $d^{(r)} = 1$ and for the left boundary $a^{(l)} = (-d - s0)$, $b^{(l)} = -(-d + s0)$, $c^{(l)} = -1$, $d^{(l)} = 1$.

The space of functions f that are analytic in the unit disk, such that the integral means

$$\int_0^{2\pi} |f(re^{i\theta})|^2 d\theta$$

are bounded as $r \to 1$ is called *Hardy* space H^2 [5] The Hardy space can be characterized as the space of functions $f(z) = \sum_{\ell=0}^{\infty} a_\ell z^\ell$ such that $\sum_{\ell=0} |a_\ell|^2$ is finite [10, III,3.4].

4. Space discretization. Space discretization is done using finite elements in the interior. Ansatz and test functions are globally continuous functions, which are piecewise polynomials. Choosing ansatz and test functions which are supported by only one single or two neighboring finite elements yields the well established sparse mass matrix M and a system matrix S. Locally on an interval (finite element) of length h for linear ansatz and test functions one obtains

$$M_{loc} = \frac{h}{6}\begin{pmatrix} 2 & 1 \\ 1 & 2 \end{pmatrix} \quad S_{loc} = \frac{1}{h}\begin{pmatrix} -1 & 1 \\ 1 & -1 \end{pmatrix} + 2d\frac{1}{2}\begin{pmatrix} -1 & 1 \\ -1 & 1 \end{pmatrix} - k^2\frac{h}{6}\begin{pmatrix} 2 & 1 \\ 1 & 2 \end{pmatrix}.$$

These have to be assembled to the global matrices M and S. In sloppy notation (neglecting boundary terms) for the interior one obtains collecting degrees of freedom into a vector $\tilde{\mathbf{u}}$

$$p(\omega)\tilde{M}\tilde{\mathbf{u}}(\omega) = \tilde{S}\tilde{\mathbf{u}}(\omega). \tag{4.1}$$

The situation at the boundary is different. The test function $v_s(x)$, which is depicted in Fig. 4.1 for the right artificial boundary point for fixed s is given by

$$v_s(x) = \begin{cases} e^{-s(x-a)} & x \geq a \\ \frac{x-(a-h)}{h} & a-h \leq x \leq a \end{cases}$$

Here $v_s(x)$ is not one function but a family of functions parameterized by s. $v_s(x)$ is globally continuous but is not finitely supported (it is supported by $[a-h, \infty)$). Assuming that $\mathbf{u}(\omega, x)$ on $[(a-h), a]$ is given as the superposition $\sum_j u_j(\omega)\phi_j(x)$ of

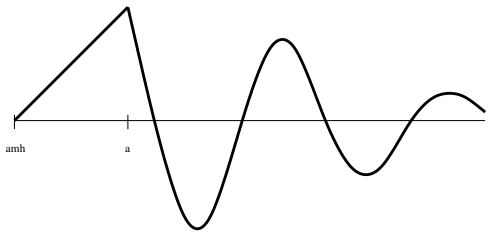

FIG. 4.1. *Boundary exp-element*

$\phi_j(x)$ – the ansatz functions ϕ_i do not vanish on $[(a-h), a]$ – the equation obtained

by testing against $v_s(x)$ is

$$\begin{aligned}
&\int_{[a-h,a]} p(\omega) \sum_j u_j(\omega)\phi_j(x)\frac{x-(a-h)}{h}\,dx + p(\omega)U^{(r)}(\omega,s) = \\
&\int_{[a-h,a]} \sum_j u_j(\omega)\left(-\phi_j'(x)\frac{1}{h} + 2d\phi_j'(x)\frac{x-(a-h)}{h} - k^2\phi_j(x)\frac{x-(a-h)}{h}\right)dx \\
&+ s(sU^{(r)}(\omega,s) - \mathbf{u}(\omega,a)) + 2d(sU^{(r)}(\omega,s) - \mathbf{u}(\omega,a)) - k^2U^{(r)}(\omega,s)
\end{aligned} \tag{4.2}$$

For the Laplace transform $U^{(r)}(\omega,s)$ of the solution $\hat{u}(\omega,x)$ in the right exterior domain the series expansion (3.10) with coefficients $a_j(\omega)$ is inserted, and the series is truncated by setting $a_\ell = 0$ for $\ell \geq L+1$. In what follows equations for the unknown coefficients $a_j(\omega)$ are derived using the PDE. The two cases $d = 0$ and $d \neq 0$ are treated separately.

Case $d = 0$. Setting

$$\hat{u}^{(0)}(a) = \sum_j \int_{[a-h,a]} u_j(\omega)\phi_j(x)\frac{x-(a-h)}{h}\,dx$$

and

$$\hat{u}^{(2)}(a) = \sum_j \int_{[a-h,a]} -u_j(\omega)\phi_j'(x)\frac{1}{h}\,dx$$

the weak form of the Neumann data can be evaluated as

$$\hat{u}'(a) = (p+k^2)\hat{u}^{(0)}(a) - \hat{u}^{(2)}(a)\ .$$

Here it is assumed without loss of generality that the initial value(s) are supported in $[-a+h, a-h]$ and that k is constant outside $[-a+h, a-h]$. With these settings (4.2) in the variable $\tilde{s}$ may be conveniently written as

$$\begin{aligned}
&p(\omega)\hat{u}^{(0)}(a) + p(\omega)U^{(r)}(\omega,\tilde{s}) = \hat{u}^{(2)}(a) - k^2\hat{u}^{(0)}(a) \\
&+ s_0(\omega)\frac{\tilde{s}+1}{\tilde{s}-1}\left(s_0(\omega)\frac{\tilde{s}+1}{\tilde{s}-1}U^{(r)}(\omega,\tilde{s}) - \mathbf{u}(\omega,a)\right) - k^2U^{(r)}(\omega,\tilde{s})
\end{aligned} \tag{4.3}$$

Multiplying by $(\tilde{s}-1)^2$ and rearranging terms yields

$$\begin{aligned}
\left(s_0^2(\omega)(\tilde{s}+1)^2 - (\tilde{s}-1)^2\left(p(\omega)+k^2\right)\right)U^{(r)}(\omega,\tilde{s}) = \\
(\tilde{s}-1)^2\hat{u}'(a) + s_0(\omega)(\tilde{s}^2-1)\mathbf{u}(\omega,a)
\end{aligned}$$

Sorting for powers of $\tilde{s}$ we obtain

$$\begin{aligned}
&\left(\left(s_0^2 - p(\omega) - k^2\right)\tilde{s}^2 + 2\left(s_0^2 + p(\omega) + k^2\right)\tilde{s} + \left(s_0^2 - p(\omega) - k^2\right)\right)U(\omega,\tilde{s}) = \\
&\tilde{s}^2\left(\hat{u}'(a) + s_0(\omega)\mathbf{u}(\omega,a)\right) - 2\tilde{s}\hat{u}'(a) + \left(\hat{u}'(a) - s_0(\omega)\mathbf{u}(\omega,a)\right)
\end{aligned}$$

Inserting the series representation (3.10) and comparing the coefficients yields

$$\left(s_0^2 - p - k^2\right)a_0 = \hat{u}'(a) - s_0\mathbf{u}(\omega,a) \tag{4.4}$$

$$2\left(s_0^2 + p + k^2\right)a_0 + \left(s_0^2 - p - k^2\right)a_1 = -2\hat{u}'(a) \tag{4.5}$$

$$\left(s_0^2 - p - k^2\right)a_0 + 2\left(s_0^2 + p + k^2\right)a_1 + \left(s_0^2 - p - k^2\right)a_2 = \hat{u}'(a) + s_0\mathbf{u}(\omega,a) \tag{4.6}$$

$$\left(s_0^2 - p - k^2\right)a_{\ell-1} + 2\left(s_0^2 + p + k^2\right)a_\ell + \left(s_0^2 - p - k^2\right)a_{\ell+1} = 0 \tag{4.7}$$

Replacing (4.6) by the sum of (4.6), (4.5) and (4.4) yields

$$4s_0^2 a_0(\omega) + \left(3s_0^2 + p(\omega) + k^2\right) a_1(\omega) + \left(s_0^2 - p(\omega) - k^2\right) a_2(\omega) = 0 \tag{4.8}$$

Equation (4.5) is replaced by (4.5) plus twice Equation (4.4) yielding

$$4s_0^2 a_0(\omega) + \left(s_0^2 - p(\omega) - k^2\right) a_1(\omega) = -2s_0 \mathbf{u}(\omega, a) \tag{4.9}$$

These equations hold for the right boundary a, with the Laplace transform taken from the boundary to ∞. With the corresponding definition of $\hat{u}^{(0)}(-a)$ and $\hat{u}^{(2)}(-a)$ we can also define $\hat{u}'(-a)$ and get identical equations for the left boundary $-a$ by using a series expansion for $U^{(l)}(\omega, \tilde{s})$.

Let us have a closer look at (4.4). So far we did not specify s_0. If we would choose $s_0(\omega)$ such that

$$s_0(\omega) = -\sqrt{k^2 + p(\omega)}\,, \quad \text{i.e. } s_0^2(\omega) - p(\omega) - k^2 \equiv 0$$

(4.4) reduces to

$$\hat{u}'(a) = s_0 \mathbf{u}(\omega, a) \Leftrightarrow -\frac{1}{\sqrt{k^2 + p(\omega)}} \hat{u}'(a) = \mathbf{u}(\omega, a) \tag{4.10}$$

which is equivalent to the exact transparent boundary conditions (2.8) or (2.9). In this case the equations for the a_ℓ are decoupled. Thus by construction we have the following theorem

THEOREM 4.1. *For the choice $s_0(\omega) = -\sqrt{p(\omega) + k^2}$ the pole condition based transparent boundary condition coincides with the classical transparent boundary condition, respectively the time discrete transparent boundary condition.*

Case $d \neq 0$ Setting additionally

$$\hat{u}^{(1)}(a) = \sum_j \int_{[a-h,a]} u_j(\omega) \phi_j'(x) \frac{x - (a-h)}{h}\, dx$$

the Neumann data is now given by

$$\hat{u}'(a) = p(\omega)\hat{u}^{(0)}(a) - \hat{u}^{(2)}(a) - 2d\hat{u}^{(1)}(a) + k^2 \hat{u}^{(0)}(a)\ .$$

(4.2) in the variable $\tilde{s}$ is conveniently written as

$$\begin{aligned} &p(\omega)\hat{u}^{(0)}(\omega) + p(\omega)U^{(r)}(\omega, \tilde{s}) = \hat{u}^{(2)} + 2d\hat{u}^{(1)} - k^2\hat{u}^{(0)} \\ &+ \frac{(s_0 - d)\tilde{s} + (d + s_0)}{\tilde{s} - 1} \left(\frac{(s_0 - d)\tilde{s} + (d + s_0)}{\tilde{s} - 1} U^{(r)}(\omega, \tilde{s}) - \mathbf{u}(\omega, a) \right) \\ &+ 2d \left(\frac{(s_0 - d)\tilde{s} + (d + s_0)}{\tilde{s} - 1} U^{(r)}(\omega, \tilde{s}) - \mathbf{u}(\omega, a) \right) - k^2 U^{(r)}(\omega, \tilde{s}) \end{aligned} \tag{4.11}$$

Multiplication by $(\tilde{s} - 1)^2$, and rearranging terms yields

$$\begin{aligned} &(\tilde{s} - 1)^2 \hat{u}'(a) + \left(s_0(\tilde{s}^2 - 1) + 2d(s - 1)^2\right) \mathbf{u}(\omega, a) = \\ &- \left((\tilde{s} - 1)^2 (p(\omega) + k^2 + d^2) - s_0^2 (\tilde{s} + 1)^2\right) U^{(r)}(\omega, \tilde{s}) \end{aligned}$$

Sorting for powers of $\tilde{s}$, inserting the series representation (3.10) and comparing the coefficients yields

$$\left(s_0^2 - d^2 - p - k^2\right) a_0 = \hat{u}' + (d - s_0)\mathbf{u}(\omega, a) \tag{4.12}$$

$$2\left(s_0^2 + d^2 + p + k^2\right) a_0 + \left(s_0^2 - d^2 - p - k^2\right) a_1 = -2(\hat{u}' + d\mathbf{u}(\omega, a)) \tag{4.13}$$

$$\begin{aligned}&\left(s_0^2 - d^2 - p - k^2\right) a_0 + 2\left(s_0^2 + d^2 + p + k^2\right) a_1 + \left(s_0^2 - d^2 - p - k^2\right) a_2 \\ &= \hat{u}' + (s_0 + d)\mathbf{u}(\omega, a)\end{aligned} \tag{4.14}$$

$$\left(s_0^2 - d^2 - p - k^2\right) a_{\ell-1} + 2\left(s_0^2 + d^2 + p + k^2\right) a_\ell + \left(s_0^2 - d^2 - p - k^2\right) a_{\ell+1}^2 = 0 \tag{4.15}$$

Replacing (4.14) by the sum of (4.14), (4.13) and (4.12) yields

$$4s_0^2 a_0 + \left(3s_0^2 + p + d^2 + k^2\right) a_1 + \left(s_0^2 - p - d^2 - k^2\right) a_2 = 0 \tag{4.16}$$

Equation (4.13) is replaced by (4.13) plus twice equation (4.12) yielding

$$4s_0^2 a_0 + \left(s_0^2 - p - d^2 - k^2\right) a_1 = -2s_0\mathbf{u}(\omega, a) \tag{4.17}$$

These equations hold for the right boundary a, with the Laplace transform taken from the boundary to ∞. Similar equations hold for the left boundary $-a$.

Collecting the $a_j(\omega)$ and the interior degrees of freedom in a vector $\underline{\mathbf{u}}$ the equation for the interior degrees of freedom (4.1) the coupling equation (4.12), the equation for a_0 (4.17), the equation for a_1 (4.16) and the equations for a_j; $2 \leq j \geq L$ (4.15) are conveniently written in matrix vector form

$$p(\omega)M\underline{\mathbf{u}}(\omega) = s_0^2(\omega)C_2\underline{\mathbf{u}}(\omega) + s_0(\omega)C_1\underline{\mathbf{u}}(\omega) + S\underline{\mathbf{u}}(\omega) \tag{4.18}$$

5. Time discretization. We use the trapezoidal rule for all equations to discretize in time.

For the Schrödinger equation, $s_0(\omega)$ is chosen to be constant $s_0 = -1 - i$. So the domain where the boundary condition requires the Laplace transform to be analytic is the set of points below the line bisecting the first and the fourth quadrant (cf. figure 3.2). After transforming back to time domain, the trapezoidal rule approximation is given by

$$iM\frac{\underline{\mathbf{u}}^{n+1} - \underline{\mathbf{u}}^n}{h} = (s_0^2 C_2 + s_0 C_1 + S)\frac{\underline{\mathbf{u}}^{n+1} - \underline{\mathbf{u}}^n}{2}$$

For the heat and drift diffusion equation, $s_0(\omega)$ is chosen to be constant $s_0 = -1$, so that poles of $U(s)$ at the right half plane of $\mathbf{C}$ are excluded (see figure 3.4). The trapezoidal rule approximation then reads

$$M\frac{\underline{\mathbf{u}}^{n+1} - \underline{\mathbf{u}}^n}{h} = (s_0^2 C_2 + s_0 C_1 + S)\frac{\underline{\mathbf{u}}^{n+1} - \underline{\mathbf{u}}^n}{2}$$

For the wave equation, we choose $s_0(\omega) = i\omega$. So when transforming back to time domain, $s_0(\omega)$ becomes ∂_t. The trapezoidal rule yields

$$(M + C_2)\frac{\underline{\mathbf{u}}^{n+1} - 2\underline{\mathbf{u}} + \underline{\mathbf{u}}^{n-1}}{h^2} = C_1\frac{\underline{\mathbf{u}}^{n+1} - \underline{\mathbf{u}}^{n-1}}{2h} + S\frac{\underline{\mathbf{u}}^{n+1} + 2\underline{\mathbf{u}} + \underline{\mathbf{u}}^{n-1}}{4}$$

Using the leap-frog scheme one alternatively obtains

$$(M + C_2)\frac{\underline{\mathbf{u}}^{n+1} - 2\underline{\mathbf{u}} + \underline{\mathbf{u}}^{n-1}}{h^2} = C_1\frac{\underline{\mathbf{u}}^{n+1} - \underline{\mathbf{u}}^{n-1}}{2h} + S\underline{\mathbf{u}}^n$$

6. Numerical examples.

6.1. Schrödinger equation. The analytical solution for the Schrödinger equation $ic\partial_t u = \partial_{xx} u$, describing a single Gaußian beam that is traveling to the left or right with an angle r, is given by

$$u_p(x,t) = \sqrt{\frac{ci}{4t+ci}} \exp\left(\frac{-ci(x-x_0)^2 - cp(x-x_0) - p^2 t}{4t+ci}\right),$$

with $p = c/2\tan(r)$, $r \in [-\pi, \pi]$. In the example a superposition of three such beams is used. Hence the initial data is $u(x,0) = u_{p_1}(x,0) + u_{p_2}(x,0) + u_{p_3}(x,0)$ with angles given by $r_1 = 5/6\pi$, $r_2 = -5/7\pi$ and $r_3 = -5/8\pi$. The analytic solution is thus given by

$$u_{\text{ref}}(x,t) = u_{p_1}(x,t) + u_{p_2}(x,t) + u_{p_3}(x,t).$$

The spatial l_2 error at $t = nh$ is defined by

$$e^n = \left((\tilde{\mathbf{u}}^n - \Pi u_{\text{ref}}(x,nh))^T \tilde{M} (\tilde{\mathbf{u}}^n - \Pi u_{\text{ref}}(x,nh))\right)^{1/2} \tag{6.1}$$

where $\tilde{\mathbf{u}}^n$ is the coefficient vector of the finite element solution at time level n, $\tilde{M}$ is the mass matrix and Π is the projection operator onto the finite element space. For $c = 4$

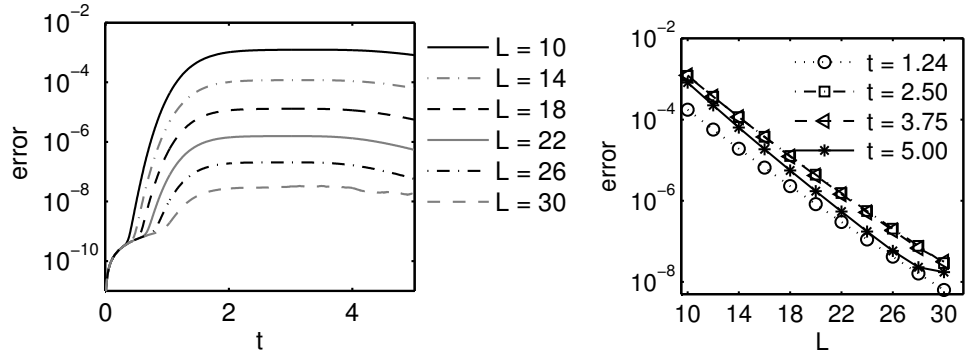

FIG. 6.1. *Left:Spatial l_2 error over time for different L for quadratic FEM with $\Delta x = 1/500$ and $h = 5 \cdot 10^{-6}$. Right: Spatial l_2 error e^n at different times $t = nh$ versus L for quadratic FEM with $\Delta x = 1/500$ and $h = 5 \cdot 10^{-6}$.*

the Schrödinger equation is integrated from $t = 0, \ldots, 5$. The computational domain is the interval $[-5, 5]$. The angles are chosen such that the maximum of the fastest traveling beam reaches the boundary at about $t = 2$. The parameter in the Möbius transform is $s_0 = -1 - i$ and we didn't try to optimize this choice. In the experiments shown in Fig. 6.1 second order finite elements (quadratic ansatz functions) where used. The mesh-width is $\Delta x = 1/500$ and the step size $h = 5 \cdot 10^{-6}$. The left subplot shows the evolution of the error for various numbers of coefficients in the power series (3.10). In the left of Fig. 6.1 at about $t = 1$ the error increases drastically if only few coefficients in the power series are used. This is due to the truncation error, which introduces reflections at the boundary, which are large for small values of L. In the right sub plot the error is shown for several fixed t. This plot indicates that the truncation error introduced decays super algebraic or even exponentially in the

number of coefficients in the power series. This is an excellent result. With just a few additional degrees of freedom, a good quality transparent boundary condition is obtained. One has to compare the 30 additional degrees of freedom with the 10000 degrees of in the interior, that are necessary to attain an error of 10^{-7}, cf. Fig. 6.2. In

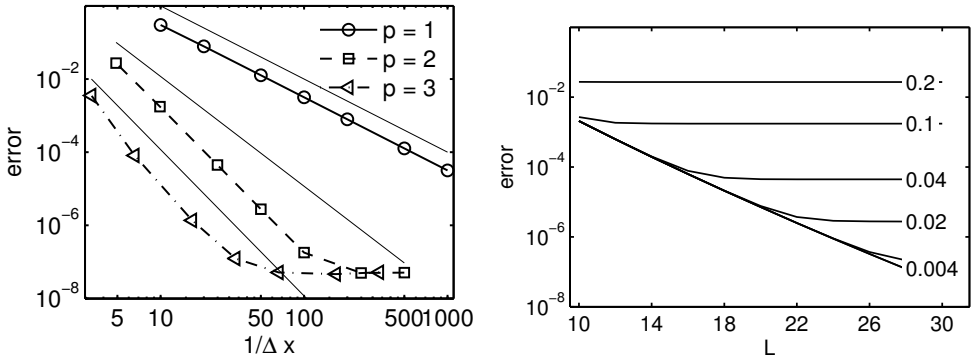

FIG. 6.2. *Left: Spatial and temporal l_2 error versus the the spatial mesh-width Δx. As a guide to the eye lines with slope -2, -3, and -4 are included. Right: Spatial and temporal l_2 error versus L for different Δx obtained with quadratic FEM and $h = 5 \cdot 10^{-6}$.*

Fig. 6.2 the l_2 error with respect to time and space ($e = \sum_n he^n$) is shown. The left plot shows the error versus Δx for first, second and third order finite elements. The linear finite elements show the expected second order convergence. Second order finite elements show a fourth order convergence, which is one order better than expected. Third order finite elements show a convergence that is slightly better than may be expected. As a guide to the eye thin lines with a slope of -2, -3 and -4 are inserted. The number of coefficients in the power series is $L = 30$, and the temporal step-size is $h = 5 \cdot 10^{-6}$. The right plot shows the error versus L for various Δx for quadratic finite elements. This shows for example that for $\Delta x = 0.04$ the error saturates with $L = 16$.

6.2. Heat equation. The fundamental solution of the heat equation $\partial_t u = \partial_{xx} u$ is

$$u(x,t) = \exp\left(-\frac{1}{2\sqrt{\pi t}}\frac{(x-x_0)^2}{4t}\right).$$

The heat equation is integrated form $t = 0.02, \ldots, 5$ on the interval $[-5,\ 5]$. In the simulation the initial data is given by $u_0(x) = u(x, 0.02)$. Again the l_2 error e^n at $t_0 + nh$ is defined by (6.1) with $u_{\text{ref}}(x, t_0 + nh) = u(x, t_0 + nh)$. The parameter for the Möbius transform is $s_0 = -1$. In the experiments shown in Fig. 6.3 quadratic finite elements where used. The mesh-width is $\Delta x = 1/250$ and the step size $h = 10^{-5}$. In the right sub plot the error is shown for several fixed t. Again this plot indicates that the truncation error introduced decays super algebraic or exponentially in the number of coefficients in the power series. The left sub-plot shows the evolution of the error for various numbers of coefficients in the power series (3.10). In Fig.6.4 the l_2 error with respect to time and space ($e = \sum_n he^n$) is shown. The left plot shows the error versus Δx for first, second and third order finite elements. The linear finite elements show the expected second order convergence. Again second and third order finite elements show a fourth order convergence. We assume that the unexpectedly good

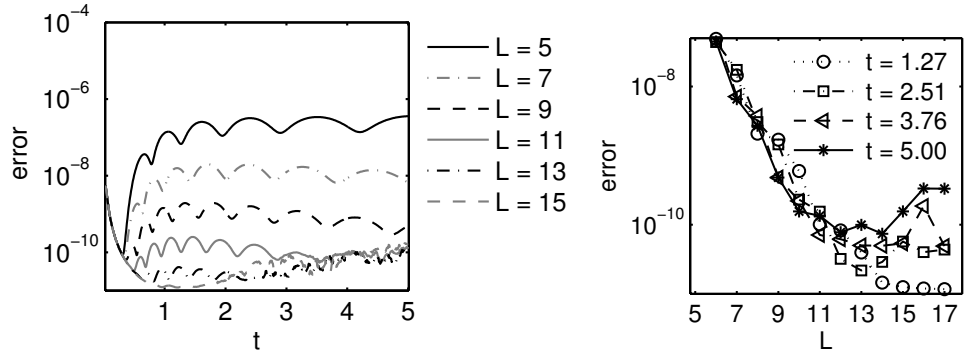

FIG. 6.3. *Left: Spatial l_2 error e^n at different times $t = nh$ versus L for quadratic FEM with $\Delta x = 1/250$ and $h = 10^{-5}$. Right: Evolution of the error for different L for quadratic FEM with $\Delta x = 1/250$ and $h = 10^{-5}$.*

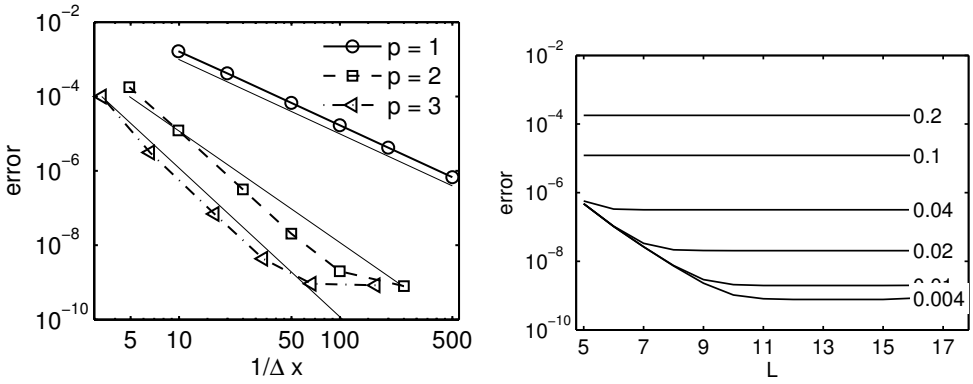

FIG. 6.4. *Left: Spatial and temporal l_2 error versus the the spatial mesh-width Δx for $h = 10^{-5}$ and $L = 17$. Right: Spatial and temporal l_2 error versus L for different Δx obtained with quadratic FEM and $h = 10^{-5}$.*

convergence property of the second order finite elements is due to some symmetry in this very solution. The number of power series coefficients is $L = 17$, and the temporal step-size is $h = 10^{-5}$. The right plot shows the error versus L for various Δx for quadratic finite elements.

6.3. Drift diffusion equation. The fundamental solution for the drift diffusion equation $\partial_t u = \partial_{xx} u + 2\partial_x u$ is given by

$$u(x,t) = \exp\left(-\frac{1}{\sqrt{4\pi t}}\frac{(x - x_0 + 2t)^2}{4t}\right).$$

We set the initial time to 0.2, $x_0 = 1$ and use $u_0(x) = u(x, 0.2)$ as initial data to integrate the drift diffusion equation from $t = 0.2, \ldots 3$ on the interval $[-5,\ 5]$. Again the l_2 error e^n at $t_0 + nh$ is defined by (6.1) with $u_{\text{ref}}(x, t_0 + nh) = u(x, t_0 + nh)$. The results are almost identical to the ones obtained for the heat equation. In the experiments shown in Fig. 6.5 quadratic finite elements where used. The mesh-width is $\Delta x = 1/400$ and the step size $h = 10^{-5}$. The left sub-plot shows the evolution of the error for various numbers of coefficients in the power series (3.10). The parameters

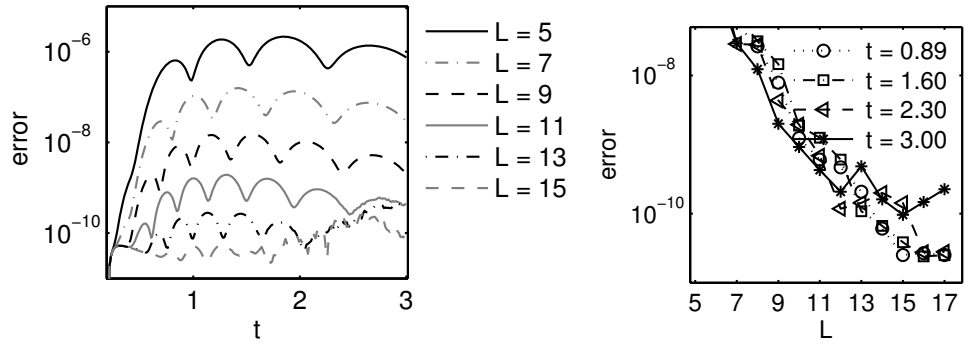

FIG. 6.5. *Left: Spatial l_2 error e^n at different times $t = nh$ versus L for quadratic FEM with $\Delta x = 1/400$ and $h = 10^{-5}$. Right:Spatial l_2 error over time for different L for quadratic FEM with $\Delta x = 1/400$ and $h = 10^{-5}$.*

are such that the maximum of the solution hits the boundary at about $t = 2.6$. In the right sub plot the error is shown for several fixed t. Again this plot indicates that the truncation error introduced decays super algebraic or exponentially in the number of coefficients in the power series.

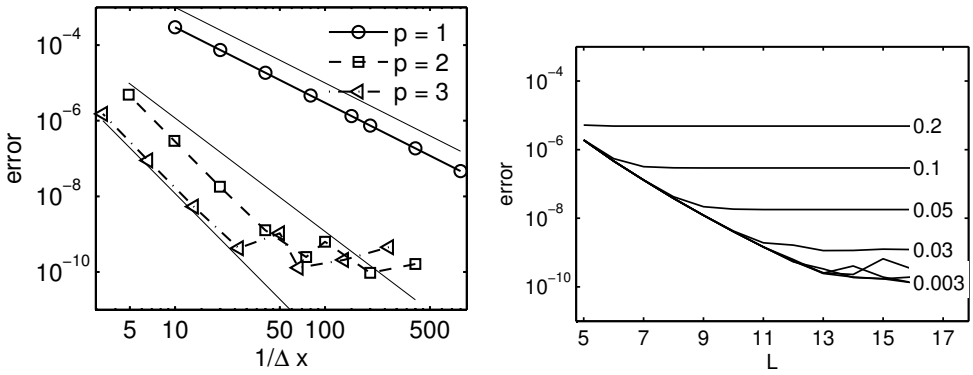

FIG. 6.6. *Left: Spatial and temporal l_2 error versus the the spatial mesh-width Δx. Right: Spatial and temporal l_2 error versus L for different Δx obtained with quadratic FEM and $h = 10^{-5}$.*

In Fig.6.6 the l_2 error with respect to time and space ($e = \sum_n he^n$) is shown. The left plot shows the error versus Δx for first, second and third order finite elements. The linear and third order finite elements show the expected second order and fourth order convergence. Second order finite elements show a again a convergence that is better than may be expected. The number of power series coefficients is $L = 17$, and the temporal step-size is $h = 1e - 5$. The right plot shows the error versus L for various Δx for quadratic finite elements.

6.4. Wave equation. The initial data for the wave equation is a Gaussian $u^0(x) = \exp\left(x^2\right)$ centered around 0 The initial velocity is set to 0, which is approximated by setting $\tilde{\mathbf{u}}^{-1} = \tilde{\mathbf{u}}^0 + h^2/2(\tilde{S}\tilde{\mathbf{u}}^0)$ in the algorithm. As there is no analytic reference solution available for the damped wave equation, a reference solution $\tilde{\mathbf{u}}^n_{\text{ref}}$ is computed on a three times larger domain, i.e $m = -3M, \ldots, 3M$, using the same Δx

and h. The error is measured in the energy norm given by

$$e^n = \frac{1}{2}(\tilde{\mathbf{e}}_t^n)^T \tilde{M}(\tilde{\mathbf{e}}_t^n) + (\tilde{\mathbf{e}}^n)^T \tilde{A}(\tilde{\mathbf{e}}^n), \tag{6.2}$$

where $\tilde{\mathbf{e}}_t = (\tilde{\mathbf{e}}^{n+1} - \tilde{\mathbf{e}}^{n+1})/2/h$ is an approximation to the velocity, and $\tilde{M}$ and $\tilde{A}$ are the mass and stiffness matrix in the interior domain. The error vector is given by $\tilde{\mathbf{e}}^n = \tilde{\mathbf{u}}^n - P\tilde{\mathbf{u}}^n_{\text{ref}}$, where $P\tilde{\mathbf{u}}^n_{\text{ref}}$ is the restriction of the reference solution to the degrees of freedom corresponding to the computational domain.

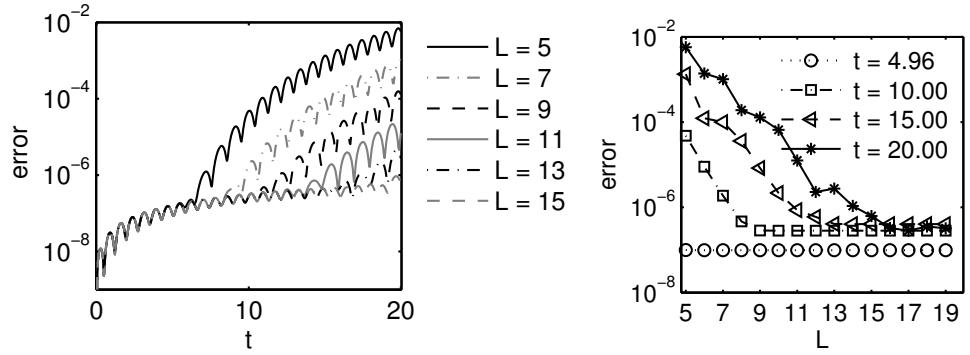

FIG. 6.7. *Left: Error e^n (6.2) at different times $t = nh$ versus L for quadratic FEM with $\Delta x = 1/250$ and $h = 5 \cdot 10^{-5}$. Right: Error in energy norm over time for different L for quadratic FEM with $\Delta x = 1/250$ and $h = 5 \cdot 10^{-5}$.*

In Fig. 6.7 the discretization parameters are $\Delta x = 1/250$ and $h = 5 \cdot 10^{-5}$; second order finite elements were used. The left sub-plot shows the evolution of the error for L ranging from 5 to 15. In the beginning the error is very small as we are not measuring any Δx or h dependent discretization error, but solely the error introduced by the discretization of the boundary condition. The right sub-plot displays the error measured at about $t = 4.96, 10, 15, 20$ for different number of coefficients L in the power series expansion. In Fig. 6.8 we have plotted the error over Δx for linear,

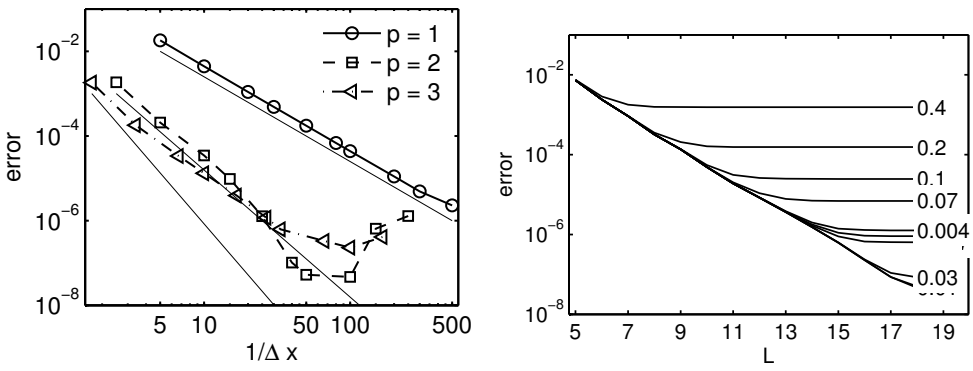

FIG. 6.8. *Left: Error ($e = \sum_n e^n$) over the the spatial mesh-width Δx. Right: Spatial and temporal l_2 error versus L for different Δx obtained with quadratic FEM and $h = 5 \cdot 10^{-5}$.*

quadratic and cubic finite-elements. The cubic finite elements only show a third order convergence, which is worse than one may have hoped for.

7. Summary. We presented a new general approach to construct transparent boundary conditions for the wave-, heat-, Schrödinger- and drift-diffusion equation. The central idea of the pole condition is to distinguish between incoming/unbounded and outgoing/bounded exterior solutions by looking at the poles of the spatial Laplace transform. From this analysis it could be seen that an exact transparent boundary condition requires the Laplace transform to be analytic in a certain domain in the complex plane, whereas the location of this domain depends on the equation. It was shown that the well known exact analytic TBCs are recoverd with this ansatz by a special choice of parameters. To construct a numerical algorithm, the Laplace transform was represented as a power series on the unit disc, which then allowed the derivation of equations for the coefficients. The actual scheme then computes a finite number of these coefficients, providing an approximate discrete TBC. It has been shown in numerical experiments for all four equations, that the error introduced by the boundary conditions decays exponentially fast in the number L of coefficients. As all our examples were one-dimensional, the number of unknowns added to the system in order to realize the boundary at both sides of the computational domain is $2L$. Even for very fine spatial resolution in the computational domain (order of thousands of nodes), around 20 additional unknowns were sufficient to reduce the boundary error to the order of the discretization error in the interior.

Although this paper was restricted to the one-dimensional case, the method can be extended to higher dimensions. The extension to the two- and three-dimensional case will be subject of future work.

REFERENCES

[1] A. Arnold and M. Ehrhardt, *Discrete transparent boundary conditions for wide angle parabolic equations in underwater acoustics*, J. Comp. Phys., (1998), pp. 611–638.

[2] R. Astley, *Infinite elements for wave problems: A review of current formulations and an assessment of accuracy.*, Int. J. Numer. Methods Eng., 49 (2000), pp. 951–976.

[3] J.-P. Bérenger, *A perfectly matched layer for the absorption of electromagnetic waves*, J. Comput. Phys., 114 (1994), pp. 185–200.

[4] W. C. Chew and W. H. Weedon, *A 3-d perfectly matched medium for modified Maxwell's equations with stretched coordinates*, Micr. Opt. Tech. Lett., 7 (1994), pp. 599–604.

[5] P. Duren and A. Schuster, *Bergman Spaces.*, Mathematical Surveys and Monographs 100. Providence, RI: American Mathematical Society (AMS)., 2004.

[6] T. Hagstrom, *Radiation boundary conditions for numerical simulation of waves*, Acta Numerica, 8 (1999), pp. 47–106.

[7] T. Hagstrom, *New results on absorbing layers and radiation boundary conditions.*, in Ainsworth, Mark (ed.) et al., Topics in computational wave propagation. Direct and inverse problems. Berlin: Springer. Lect. Notes Comput. Sci. Eng. 31, 1-42 , 2003.

[8] E. Hairer and G. Wanner, *Solving Ordinary Differential Equations I*, Springer Verlag, Berlin, Heidelberg, 1991.

[9] T. Hohage, F. Schmidt, and L. Zschiedrich, *Solving Time-Harmonic Scattering Problems Based on the Pole Condition I: Theory*, SIAM J. Math. Anal., 35 (2003), pp. 183–210.

[10] Y. Katznelson, *An introduction to Harmonic Analysis*, Dover Publications, New York, 2 ed., 1968.

[11] C. Lubich, *Convolution quadrature and discretized operational calculus I*, Numer. Math., 52 (1988), pp. 129–145 and 413–425.

[12] ———, *Convolution quadrature and discretized operational calculus II*, Numer. Math., 52 (1988), pp. 413–425.

[13] C. Lubich and A.Ostermann, *Runge-kutta methods for parabolic equations and convolution quadrature*, Math. Comput., 60 (1993), pp. 105–131.

[14] A. Schädle, *Ein schneller Faltungsalgorithmus für nichtreflektierende Randbedingungen*, dissertation, Mathematisches Institut, Universität Tübingen, Tübingen, Germany, June 2002.

[15] F. Schmidt, *Solution of Interior-Exterior Helmholtz-Type Problems Based on the Pole Condition Concept: Theory and Algorithms*, habilitation thesis, Free University Berlin, Fach-

bereich Mathematik und Informatik, 2002.
[16] ———, *Pole Condition: A new approach to solve scattering problems*, in Oberwolfach Report, no. 1 in 1, Mathematisches Forschungsinstitut Oberwolfach, 2004, pp. 615–617.
[17] F. Schmidt and D. Yevick, *Discrete transparent boundary conditions for Schrödinger-type equations*, J. Comput. Phys., 134 (1997), pp. 96–107.
[18] S. Tsynkov, *Numerical solution of problems on unbounded domains. A review*, Applied Numerical Mathematic, 27 (1998), pp. 465–532.